CHEMISTRY

Enhancing hydrogenation activity of Ni-Mo sulfide hydrodesulfurization catalysts

Manuel F. Wagenhofer, Hui Shi*, Oliver Y. Gutiérrez†, Andreas Jentys, Johannes A. Lercher*

Unsupported Ni-Mo sulfides have been hydrothermally synthesized and purified by HCl leaching to remove Ni sulfides. Unblocking of active sites by leaching significantly increases the catalytic activity for dibenzothiophene hydrodesulfurization. The site-specific rates of both direct (hydrogenolytic) and hydrogenative desulfurization routes on these active sites that consist of coordinatively unsaturated Ni and sulfhydryl groups were identical for all unsupported sulfides. The hydrogenative desulfurization rates were more than an order of magnitude higher on unsupported Ni-Mo sulfides than on Al_2O_3-supported catalysts, while they were similar for the direct (hydrogenolytic) desulfurization. The higher activity is concluded to be caused by the lower average electronegativity, i.e., higher base strength and polarity, of Ni-Mo sulfides in the absence of the alumina support and the modified adsorption of reactants enabled by multilayer stacking. Beyond the specific catalytic reaction, the synthesis strategy points to promising scalable routes to sulfide materials broadly applied in hydrogenation and hydrotreating.

INTRODUCTION

Unsupported hydrotreating catalysts are complex mixtures of transition metal sulfides that may have synergistic and antagonistic interactions among different phases. For Mo-based catalysts, the major constituents are pure MoS_2, a Ni/Co-containing MoS_2 phase having Ni and Co incorporated at the perimeter of the MoS_2 crystals, and a variety of sulfides of Ni and Co. The promoting effects of Co and Ni are typically attributed to their selective incorporation at the MoS_2 slab edge and to the associated generation of sulfhydryl (SH) groups (*1*–*3*).

While these sites are active for hydrogenation (HYD) and hydrodefunctionalization reactions [hydrodesulfurization (HDS) and hydrodenitrogenation], nickel or cobalt metal sulfides (e.g., NiS_x) have only sites with much lower activity (*1*, *4*, *5*). Although these latter phases do not notably contribute to HYD and hydrodefunctionalization, they may adversely affect the catalytic performance by adding inert mass and blocking active sites at the MoS_2 perimeter. This complicates the evaluation of structure-function relations (*6*), as it obscures relations between chemical compositions, concentrations of active sites, and catalytic activity.

Segregation into inactive phases is especially severe for unsupported sulfides, because sulfides with high catalytic activities require concentrations of promoter metal loadings that inevitably lead to segregation into inactive phases. To unblock active sites, postsynthetic removal of the confounding phases is a promising alternative. Phase diagrams (fig. S1) indicate for Ni-Mo systems that this can be achieved via concentrated acid treatment, selectively dissolving catalytically inactive forms of Ni, whereas Ni-associated active sites and the overall catalyst structure composed of stacked MoS_2 slabs appear to be unaffected (*7*–*10*).

In the present study, we report on acid extraction as a preparative tool to obtain well-defined Ni-Mo sulfide catalysts that have an exceptionally high site-specific activity for hydrogenative desulfurization. These cleaned mixed sulfides also allow us to relate nature and concentration of active sites to catalytic properties and to corroborate recent insight into active sites (*11*).

Technische Universität München, Department of Chemistry and Catalysis Research Center, Lichtenbergstraße 4, 85748 Garching, Germany.
*Corresponding author. Email: hui.shi@mytum.de (H.S.); johannes.lercher@ch.tum.de (J.A.L.)
†Present address: Institute for Integrated Catalysis, Pacific Northwest National Laboratory, P.O. Box 999, Richland, WA 99352, USA.

RESULTS AND DISCUSSION

Selective removal of Ni sulfides

Ni-promoted parent MoS_2 catalysts were prepared via hydrothermal synthesis and were subsequently treated with concentrated HCl (pH = −1) to remove Ni sulfides (NiS_x). This treatment is named "leaching" or "acid treatment" in this paper.

Ni sulfides are not stable in highly acidic solutions (pH < 0) (*12*). We observed dissolution of NiS_x when exposing the mixed sulfide catalysts to concentrated HCl, visible by a greenish color of the solution due to the formation of aqueous Ni^{2+}, as well as by H_2S evolution. A substantial reduction (on the order of 20 to 30%) of the mass of the acid-treated catalysts was observed, while the MoS_2 component remained unmodified. This was verified by exposing MoS_2 to the identical treatment without observing significant mass loss, H_2S evolution, coloration of the solution (*13*), or a change in catalytic properties. This shows that MoS_2 is effectively inert even in strongly acidic solutions, as long as oxidants are absent (fig. S1).

X-ray diffraction (XRD) patterns before leaching (fig. S2A) show characteristic broad reflections of polycrystalline MoS_2 ($2\theta \approx 14°$, 33°, 40°, and 59°), accompanied by sharp reflections in the range of $2\theta = 27°$ to 60° assigned to Ni subsulfides Ni_3S_2 and Ni_9S_8 (*6*, *14*–*17*). An approximate calculation of the S/Ni ratio (S/Ni = 0.83 to 1.21) shows that NiS_x phases with $x > 1$ (e.g., NiS_2 and Ni_3S_4) might also be present. Note, however, that the estimated S/Ni ratio may also include (x-ray) amorphous forms of NiS_x or NiS_x present at low concentrations that are not visible by XRD.

The elemental composition (table S1) of the parent catalysts was uniform, with S/(Ni + Mo) atomic ratios of about 1.5 and Ni/(Ni + Mo) atomic ratios of 0.48 to 0.60. The composition changed substantially after exposure to concentrated HCl. The atomic metal fraction of Ni, Ni/(Ni + Mo), decreased from 0.48 to 0.60 before leaching to 0.20 to 0.26 after leaching, i.e., somewhat smaller than the typical optimum of 0.3 to 0.4 in supported sulfides (*1*, *2*, *18*). Note, however, that the Ni/(Ni + Mo) ratio in most supported catalysts

also includes Ni atoms that are not associated with MoS_2, such as cations in spinels formed with the Al_2O_3 support (*1*). The "effective" Ni/(Ni + Mo) ratio may, thus, be lower than 0.3 to 0.4 and is speculated to be close to the values of the leached catalysts.

The extensive loss of Ni (69 to 77%) was accompanied by a moderate, yet substantial, loss of sulfur (13 to 28%), whereas the concentration of Mo was not affected. These changes were also reflected in the x-ray diffractograms (fig. S2B). The NiS_x reflections disappeared almost completely, while contributions of MoS_2 remained essentially unchanged (broad reflections at $2\theta \approx 14°$, 33°, 40°, and 59°), suggesting that the structure of MoS_2 was retained after acid treatment. This is confirmed by particle size analysis via transmission electron microscopy (TEM) and XRD line broadening, which both suggest similar crystalline dimensions of the primary MoS_2 domains before and after treatment (table S1).

While the dimensions of the primary MoS_2 domains were barely affected by leaching, fundamental changes in the overall morphology were observed. Scanning electron micrographs (SEMs) of the catalysts before acid treatment showed two major structural features (Fig. 1A; see fig. S3 for supplementary micrographs). The bulk of the material consisted of rod-shaped structures of about 100 nm in diameter and 0.5 to 2 μm in length, intermixed with randomly distributed, compact particles of irregular shape and sizes no larger than 200 nm. These compact particles were absent after acid treatment (Fig. 1B), and their sizes in the parent materials agreed with those of the NiS_x domains as determined by XRD (about 75 to 150 nm). Thus, we assign the compact, irregular particles to segregated NiS_x.

Accordingly, we assign the refractory rod-like structures to a MoS_2-rich phase, likely containing the remaining Ni (Ni-Mo-S phase). The NiS_x particles visible in SEM were primary crystallites, while the rod-like MoS_2 phase is a secondary structure, composed of nanometer-sized MoS_2 domains (Fig. 1E). We would like to point out that the rod-like morphology was already present in the oxide precursors (Fig. 1D) and was retained throughout sulfidation and acid treatment. These structural features seem to be common for hydrothermally prepared MoS_2 (*14*, *19*).

In the case of NiMo-4, we observed leaching-resistant agglomerates of 10- to 50-nm particles (Fig. 1F), a structural feature that was not present in the other catalysts, in addition to the previously discussed MoS_2 rods and compact NiS_x crystals. Because of their refractory behavior in acidic solution, we conclude that the agglomerates are not entirely composed of NiS_x. We speculate that these entities are

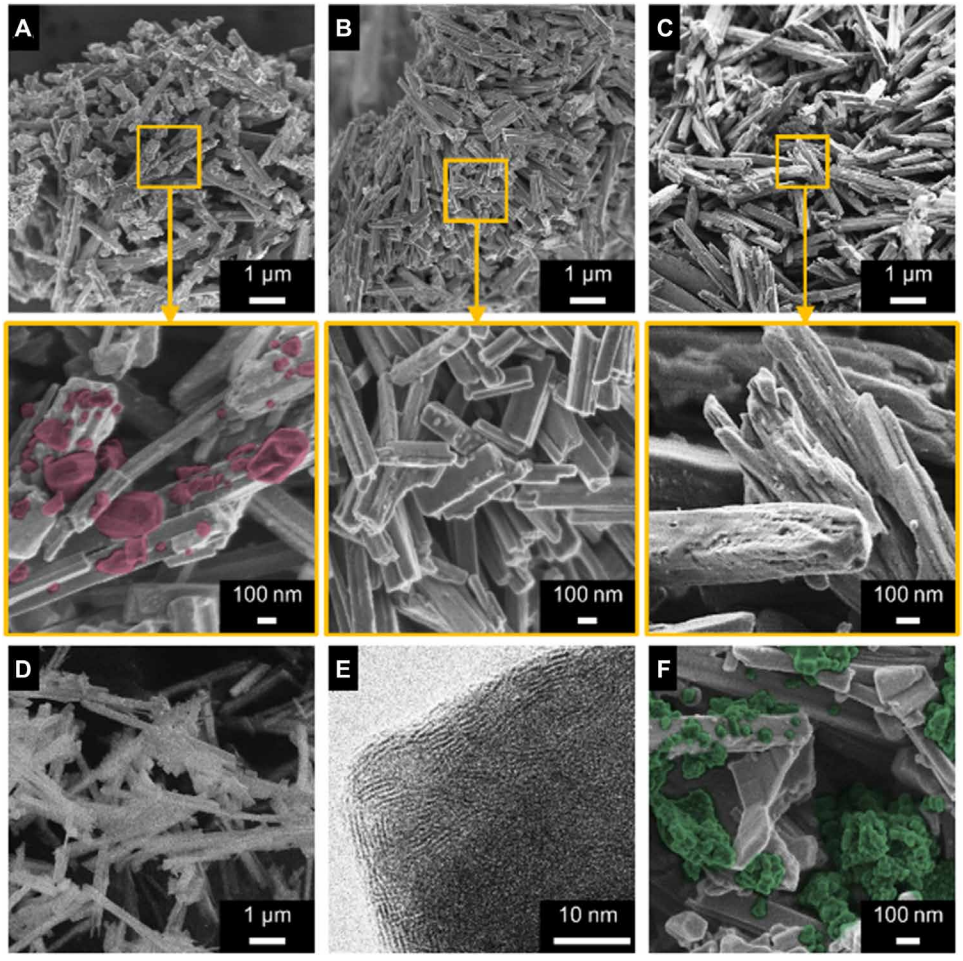

Fig. 1. Electron micrographs. (**A**) SEM of NiMo-3 before leaching with enlarged view below showing MoS_2 rods and compact NiS_x particles in false color. (**B**) SEM of NiMo-3 after leaching showing only MoS_2 rods. (**C**) SEM of NiMo-1 after leaching with enlarged view below showing corrugated surface of MoS_2 rods. (**D**) MoO_3 catalyst precursor used in hydrothermal synthesis. (**E**) Transmission electron micrograph of sulfided NiMo-3 after acid treatment. (**F**) SEM showing agglomerates of unidentified fine particles on NiMo-4 before leaching.

either MoS_2 particles with an atypical morphology or Ni sulfides encapsulated by MoS_2 (*20*).

Acid treatment led to substantially increased specific surface areas and pore volumes in the first three catalysts (table S1). This textural improvement is attributed to the uncovering of pore openings and corrugated surface regions previously blocked by NiS_x (Fig. 1C). Specific surface areas were roughly doubled by acid treatment for all but NiMo-4-p, for which specific surface area and pore volume were not significantly affected.

Based on elemental composition, XRD, TEM, and SEM, we conclude that segregated NiS_x is removed selectively without affecting the structural integrity of the MoS_2-rich constituent. We speculate that the acid-resistant Ni is incorporated in MoS_2.

Interatomic coordination

Extended x-ray absorption fine structure (EXAFS) at the Ni K-edge indicates a similar NiS_x phase mix in all of the parent catalysts (table S2), which is consistent with XRD results (table S1). Because the spectra (Fig. 2) could be modeled satisfactorily using only Ni-S and Ni-Ni scattering paths (table S3), we hypothesize that the fraction of Ni atoms in the promoted Ni-Mo-S phase is small compared to the number of Ni atoms in segregated Ni sulfides (see fig. S4 for the complete set of spectra in *k*- and *R*-space). This is supported by the analysis of chemical composition before and after leaching (table S1), which suggests that more than 70% of Ni in the parent samples is present as acid-leachable Ni sulfides. After leaching, by contrast, we found that a Mo scatterer at 2.86 Å was required to fit the data. This

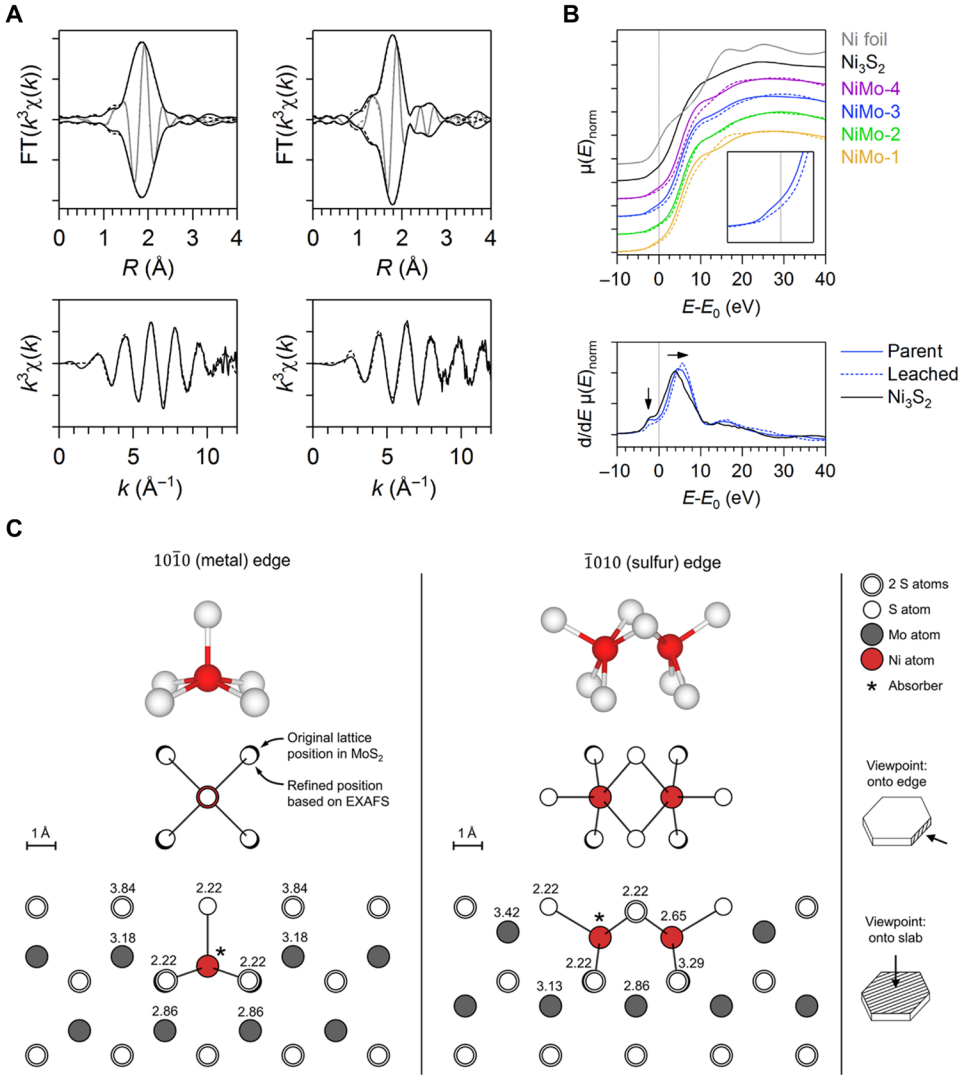

Fig. 2. Results of XAS at the Ni K-edge and structural model. (**A**) Top row: Magnitude (black) and imaginary part (gray) of the k^3-weighted Fourier transform before leaching (left) and after leaching (right) with best fit (dashed line). Bottom row: k^3-weighted EXAFS and best fit (dashed line) before (left) and after leaching (right). The distance between two vertical tick marks is 5 $Å^{-3}$ (*k*-space) and 5 $Å^{-4}$ (*R*-space). See fig. S4 for EXAFS of NiMo-1, NiMo-2, and NiMo-4. (**B**) Top: Normalized near-edge absorption (E_0 = 8333 eV) of Ni-Mo sulfide catalysts, Ni_3S_2, and Ni metal. The inset shows an enlarged view of the pre-edge. Arrows highlight features discussed in the text. Bottom: Derivative of normalized absorption of Ni_3S_2, NiMo-3-p, and NiMo-3-L. Continuous and dotted lines correspond to parent and leached samples, respectively. (**C**) Proposed local environments of Ni derived from EXAFS results. Single Ni atom incorporated at the metal edge and neighboring Ni atoms incorporated at the sulfur edge of MoS_2 shown from different perspectives [two-dimensional (2D) projections to scale, 3D representation schematic]. The numbers indicate the distance to the Ni absorber in Å (absorber denoted with asterisk).

is in good agreement with literature reports (*16*–*18*, *21*–*25*) and also with the overall picture drawn by the other characterization techniques, i.e., as most of the segregated NiS_x is removed during acidic treatment, Ni-Mo contributions from the promoted Ni-Mo-S phase become more predominant in relation to contributions from NiS_x.

In addition to the appearance of a Ni-Mo contribution, we also found that the average Ni-S distance was significantly and consistently smaller after leaching (2.22 Å compared to 2.26 Å). This distance is too short for crystalline Ni sulfides (table S3) and shows that a substantial part of the Ni atoms in acid-treated catalysts is not located in segregated NiS_x phases. In agreement with reports on supported sulfides (*21*, *23*, *24*), we conclude that the short Ni-S bonds are associated with the Ni-Mo-S phase. Figure 2C shows a possible configuration of Ni at the metal edge of MoS_2 that is consistent with the observed EXAFS parameters (see also table S2 and accompanying discussion).

Leaching-associated changes were also noticed in the Ni-Ni coordination, which appeared at a significantly larger average distance of 2.63 Å instead of 2.56 Å in the parent sulfides (table S2). The fact that Ni-Ni scattering was still observed after leaching could indicate that some NiS_x phases persisted after HCl treatment. On the other hand, Ni-Ni scattering is not necessarily associated only with segregated Ni sulfides and could also originate from neighboring Ni atoms in Ni-Mo-S. One example of a dinuclear Ni-Ni entity that is consistent with the present EXAFS analysis is shown in Fig. 2C for the sulfur edge (see also table S2 and accompanying discussion). Based on density functional theory calculations, these Ni-Ni pairs were proposed and predicted to be stable (*26*, *27*). The suggested structure at the sulfur edge closely resembles the main structural motif of naturally occurring NiS ("Millerite").

Analysis of the near-edge structure (x-ray absorption near-edge structure) highlighted further important differences between parent and leached sulfides. Both the intensity of the pre-edge feature (1s-3d transition) and the edge energy were found to qualitatively correlate with the NiS_x content (Fig. 2B). The pre-edge signal at approximately 8332 eV was most intense in the Ni_3S_2 reference, followed by the parent catalysts, and finally by the leached catalysts, in which it was barely noticeable. This sequence reflects the fact that tetrahedrally coordinated Ni, such as in Ni_3S_2, typically exhibits a more intense pre-edge than Ni in Ni-Mo-S (*24*). The gradual weakening of the pre-edge in the sequence Ni_3S_2 > NiMo-p > NiMo-L was accompanied by a blue shift in the edge energy following the same sequence and pointed to changes in the overall electron density of Ni. The gradual shift suggests that the average oxidation state of Ni increases as edge-incorporated Ni atoms become more and more significant in concentration compared to NiS_x (a mixture of phases with formal oxidation states +1.3 to +2).

Distribution of Ni among active and inactive phases

To analyze the distribution of Ni among active (Ni-Mo-S) and inactive (NiS_x) phases, we compare the total Ni content to the maximum concentration of Ni that could be theoretically incorporated at the edges (Fig. 3E). The latter is given by the number of edge metal atoms and may be estimated from TEM data using a geometric model (see Supplementary Methods). The analysis of the parent catalysts shows that much more Ni is present than potential sites that exist at MoS_2 edges (Fig. 3E). Even after acid treatment, the residual amount of Ni exceeds that of available edge positions. If we further consider that usually not all edge sites can be occupied by Ni, the discrepancy becomes even more pronounced. Thus, we reason that leached catalysts also contain some segregated Ni sulfides or small NiS_x clusters.

Thus, we conclude that the removal of NiS_x was not quantitative. This raises the question about the nature of these acid-resistant NiS_x phases. While XRD showed that Ni sulfides were absent after leaching (fig. S2), the remaining NiS_x might exist as x-ray amorphous

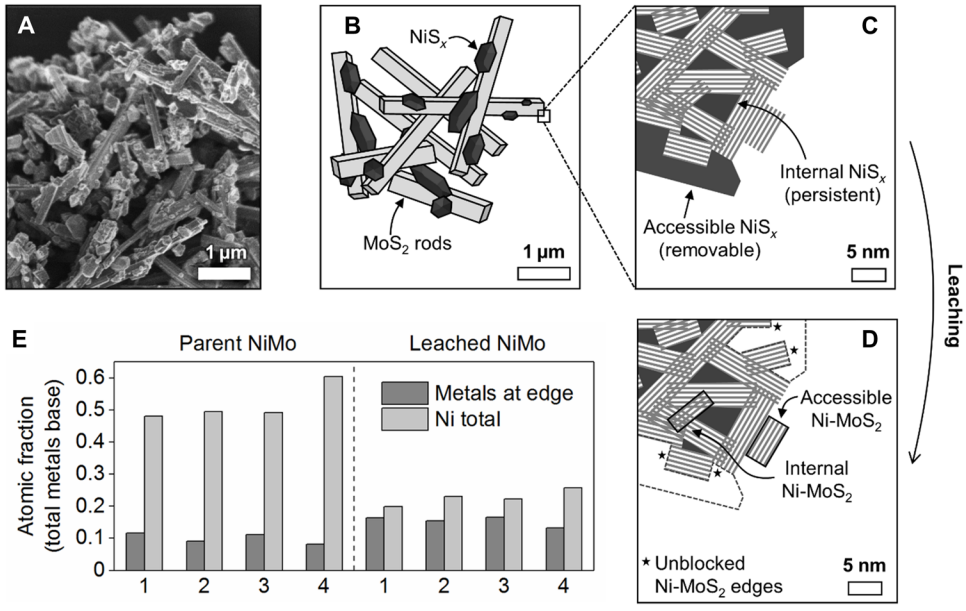

Fig. 3. Ni distribution among active and inactive phases. (**A**) Representative SEM micrograph and (**B**) schematic representation of NiMo-3 before leaching, showing secondary rod-like MoS_2 phase intermixed with crystalline NiS_x. (**C**) Enlarged cross section of the corner of one rod-like particle before leaching. (**D**) Cross section after leaching. (**E**) Comparison of total amount of Ni present in the catalysts ("Ni total" determined via elemental analysis) with amount of available edge positions ("Metals at edge" determined via TEM) before and after leaching.

domains. However, as Ni sulfides are readily soluble in concentrated HCl, these acid-resistant NiS_x phases are concluded to be at inaccessible locations, for example, within the rod-like structures (Fig. 3, A to D) or in the form of MoS_2-coated particles (*5*). Being confined by the densely packed MoS_2 matrix, the size of such NiS_x domains may be rather small. EXAFS of leached samples (table S2) supports the hypothesis of internal NiS_x reservoirs by showing a Ni-Ni contribution similar to that of bulk Ni sulfides.

Having hypothesized that internal NiS_x phases may be present after leaching, we are now in a position to estimate their proportion among the pool of Ni species (see Supplementary Methods and discussion of table S4). For this, we compare the amount of edge-incorporated Ni to the total amount of Ni in the catalysts. We used nitric oxide (NO) chemisorption to determine the concentration of Ni atoms at the accessible surface, which we then extrapolated to the inaccessible bulk of the material. The implicit assumption is that NO adsorbs predominantly on Ni-associated edge sites and that MoS_2 domains in the bulk ("internal MoS_2"; Fig. 3D) have the same degree of edge substitution by Ni as those at the accessible surface ("accessible MoS_2"; Fig. 3D). The results suggest that 24 to 40% of Ni atoms in the leached catalysts are incorporated in Ni-Mo-S (table S4), while the remainder of 60 to 76% exists as inaccessible NiS_x. The corresponding figures for the parent catalysts indicate a much lower incorporation of Ni, with only 8 to 10% of all Ni atoms located at MoS_2 edges. This is fully consistent with the conclusions from EXAFS, suggesting that the contribution of edge-incorporated Ni atoms before leaching was masked by the much more predominant NiS_x phase mix.

As for the degree of edge substitution by Ni, we determined values of 31 to 43% for three of the leached catalysts, which is in good agreement with typical maxima reported in the literature (*28*, *29*). In the case of NiMo-4-L, the calculated edge substitution degree was substantially higher than in the other catalysts (78%). Alternatively, this large value could indicate that the fraction of edge metal atoms (derived from TEM) was underestimated because particularly small MoS_2 particles may be present in this material. Figure 1F shows a very heterogeneous distribution of secondary structures, i.e., rods and agglomerates, for this particular sample.

Dibenzothiophene hydrodesulfurization

Having shown that accessible Ni sulfides are removed selectively by acid treatment, we now discuss its catalytic consequences for the HDS of dibenzothiophene (DBT). The conversion of DBT follows two distinct pathways, HYD and hydrogenolysis [also referred to as direct desulfurization (DDS) (*1*, *30*–*32*)]. In DDS, C-S hydrogenolysis to biphenyl (BP) takes place first and aromatic ring saturation occurs later. In the HYD route, the initial step consists of a gradual saturation of one aromatic ring to yield 1,2,3,4-tetrahydro-DBT and 1,2,3,4,4a,9b-hexahydro-DBT (4HDBT and 6HDBT, respectively). This is followed by hydrogenolysis of the C-S bond to cyclohexyl benzene (CHB), which is then hydrogenated to the final product bicyclohexyl (BCH). Note that this sequence may contain other (short-lived) intermediates, such as the reactive thiol (CHB-SH) shown in Fig. 4A, which we directly observed via mass spectrometry. Dihydrodibenzothiophenes [a possible class of intermediates involved in both HYD and DDS (*33*)] or 2-biphenylthiol [an intermediate formed after the cleavage of the first C-S bond along the DDS path (*33*)] was not detected.

The main products under most conditions were BP and CHB. Relevant concentrations of partially hydrogenated intermediates (4HDBT and 6HDBT) were only observed at low conversions and temperatures <290°C, while the fully saturated product, BCH, was never observed in significant concentrations. On parent and leached MoS_2, we also observed a CHB-SH intermediate (with the SH group at the aromatic ring) at low conversions and temperatures. The parent catalysts converted DBT predominantly via the HYD pathway (Fig. 4B). With increasing temperature, the selectivity to DDS increased substantially but never exceeded that of HYD. This preference contrasts that observed for supported catalysts [e.g., ~90% DDS and ~10% HYD on a sulfided Ni-Mo/Al_2O_3 sample; see table S5; see also (*33*–*35*)].

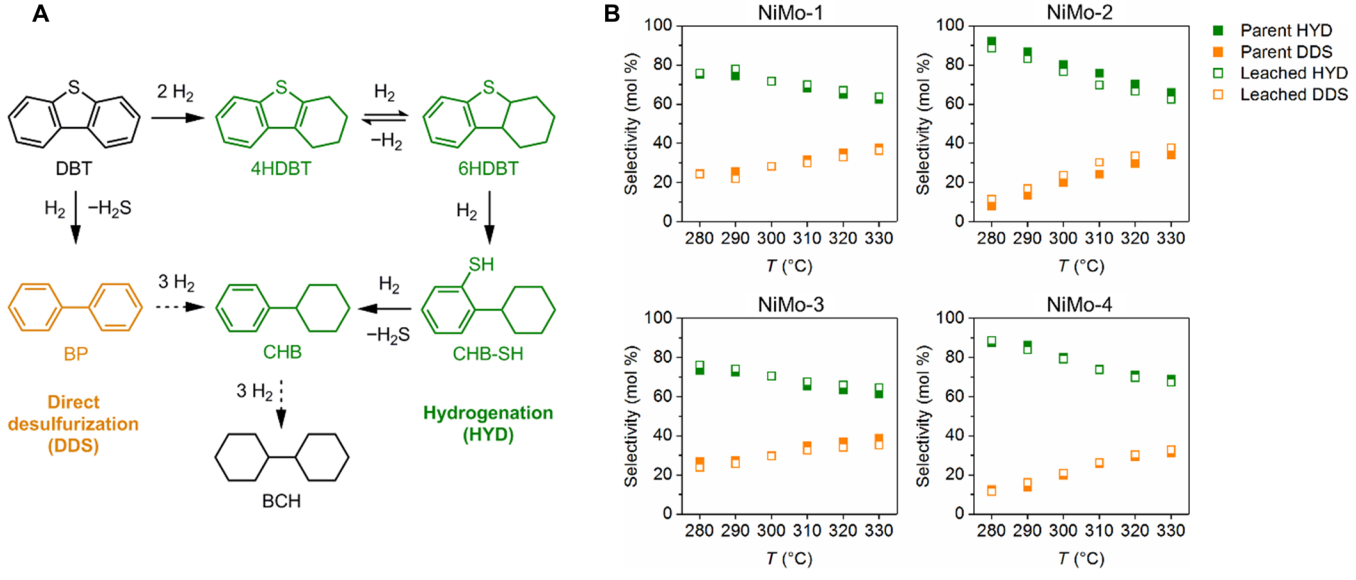

Fig. 4. DBT HDS network and measured selectivities. (**A**) Reaction network. (**B**) Selectivity for DDS and HYD of DBT on Ni-Mo sulfide catalysts before and after acid treatment as a function of temperature [trickle-bed reactor, 280° to 330°C, 5.0 MPa total pressure (H_2), 1 weight % DBT in decalin, gas/liquid = 500 Nm^3/Nm^3, weight hourly space velocity = 1]. mol %, mole percent.

Varying the residence time at 330°C resulted in constant DDS and HYD selectivity over the whole range of DBT conversions (<45%) on MoS_2 and Ni-Mo sulfides (fig. S5). Thus, the product distribution in the present analysis only depends on the temperature and is not affected by the simultaneous changes in DBT conversion, i.e., the selectivities of different catalysts at a specific temperature can be compared directly.

The product distribution in the whole temperature range was very similar on all parent Ni-Mo sulfide catalysts (for example, S_{HYD} = 62 to 69% and S_{DDS} = 31 to 38% at 330°C). This implies a similar composition of active sites, i.e., a similar distribution of Ni among DDS- and HYD-selective sites. At the same time, however, substantial differences in the distribution of Ni among active (edge-incorporated Ni) and inactive (NiS_x) phases must exist. We conclude this from the considerable variations in HDS activity (r_{HDS} = 1.5 to 6.9 mmol g^{-1} $hour^{-1}$; Table 1), which does not track the almost constant Ni content (7.0 to 8.8 atomic %; table S1). This discrepancy arises because mass-specific activity is determined not only by the concentration of incorporated Ni but also by the proportion of inert mass (NiS_x) and to the extent NiS_x blocks active sites.

The mass-specific rate increased by a factor of 1.6 to 2.3 after leaching, which exceeds the sole effect of mass loss (fig. S6A). Assuming that all sites are equally active, we estimate the fraction of sites blocked by NiS_x in the parent catalysts to be between 0.05 and 0.46. A correlation between the fraction of removed mass and the extent of site unblocking was not observed (fig. S6B).

Despite the marked effect on reaction rates, the product distribution was essentially unchanged after acid treatment (Fig. 4B), which implies that DDS and HYD pathways were enhanced by the same factor. This leads to the conclusion that newly exposed and preexisting active sites are identical. Acid leaching also did not significantly alter activation energies (E_A), as shown in the parity plot in fig. S7.

Activation energies (Table 1) for the HYD pathway were consistently lower than those of the DDS pathway, which agrees with the fact that the rate-determining step differs between the two pathways. It is noteworthy that $E_{A,HYD}$ was nearly identical, whereas $E_{A,DDS}$ showed considerable variations among different catalysts (Table 1). While the $E_{A,HYD}$ values (134 to 139 kJ mol^{-1}) indicate a corresponding uniformity of HYD-selective sites, the $E_{A,DDS}$ values vary in a relatively broad range, as multiple types of DDS sites differing in the steric environment and the basicity of the remaining S^{2-} anions in the vicinity of the vacancy exist at S- and Mo-edges (*36*). More studies are, however, needed to differentiate between these two options.

Structure-activity relations

Despite the complexity of active sites, agreement exists on the key roles of coordinatively unsaturated sites (CUS; or "sulfur vacancies") and SH groups. The most important function of CUS is to coordinate with the organic sulfur [σ or η^1(S) adsorption for DDS of less sterically hindered S-containing molecules] while also providing a pathway for activating hydrogen and transiently forming SH. Hydrogen is provided by nearby SH groups for both DDS and HYD (*37*). We have recently highlighted the direct role of SH groups in aromatics HYD over supported sulfides and found that SH groups associated with Ni edge atoms exhibited a constant intrinsic activity independent of the overall composition of the catalyst (*11*). Applying this analysis, CUS and SH groups were quantified using NO chemisorption and steady-state H_2/D_2 isotopic exchange. We would like to point out that SH groups present under the conditions of NO chemisorption are likely to undergo NO/SH exchange and, thus, be titrated along with CUS. In the following, we choose to include these SH groups, converted to CUS, in the total CUS count unless otherwise specified. Total CUS concentration was calculated directly from NO uptake assuming dinitrosyl-type adsorption (*38*, *39*), whereas SH concentration is represented indirectly by a proportional quantity, that is, H_2/D_2 isotopic exchange rates (IERs). Note that H/D exchange is directly involving SH, but CUS are part of the catalytically active site (*40*). Both methods are discussed in more detail in connection with table S6 and fig. S8.

The linear correlation between CUS concentrations and the IER values observed for the leached series of catalysts (Fig. 5A) indicates that CUS are needed for H/D exchange. The absence of such a functional dependency for the parent samples demonstrates that a major

Table 1. Initial DDS and HYD reaction rates and apparent energies of activation.

Catalyst	Initial rates (mmol g^{-1} h^{-1} or mol mol_{Mo}^{-1} $hour^{-1}$)*			E_A (kJ mol^{-1})†		
	Total	DDS	HYD	Total	DDS	HYD
NiMo-1-p	1.5 (0.36)	0.58 (0.14)	0.96 (0.22)	152 ± 4	177 ± 4	140 ± 5
NiMo-2-p	1.4 (0.34)	0.46 (0.12)	0.89 (0.22)	164 ± 5	239 ± 12	145 ± 6
NiMo-3-p	2.6 (0.49)	1.0 (0.19)	1.6 (0.30)	153 ± 10	176 ± 12	142 ± 9
NiMo-4-p	6.9 (2.02)	2.1 (0.63)	4.7 (1.39)	151 ± 4	205 ± 9	136 ± 4
MoS_2-p	2.5 (0.39)	0.46 (0.07)	2.0 (0.32)	–	–	–
NiMo-1-L	2.3 (0.41)	0.83 (0.15)	1.5 (0.26)	147 ± 5	174 ± 8	135 ± 5
NiMo-2-L	2.9 (0.53)	1.1 (0.20)	1.8 (0.33)	157 ± 5	220 ± 12	138 ± 5
NiMo-3-L	4.5 (0.86)	1.6 (0.30)	2.9 (0.56)	144 ± 3	170 ± 5	134 ± 3
NiMo-4-L	11.0 (2.23)	3.7 (0.73)	7.7 (1.50)	156 ± 4	214 ± 8	139 ± 4
MoS_2-L	2.4 (0.39)	0.41 (0.07)	2.0 (0.32)	–	–	–

*Initial rates (±5%) at 330°C; values outside and in the parentheses are normalized to the catalyst mass and to the total amount of Mo, respectively.
†Temperature range: 280° to 330°C.

fraction of CUS exist in an environment that does not have a large concentration of SH groups. We surmise that these are a fraction of CUS in NiS_x. The direct proportionality suggests a fixed ratio between CUS and SH sites in the treated samples, as we have also observed with supported sulfide catalysts (*11*). Therefore, we used the CUS concentration (half of NO uptake) as a quantity for the concentration of active sites in the studied materials while noting that some of the CUS from nonpromoted sites contribute only to a minor extent to DDS and HYD activities.

Figure 5B shows DDS and HYD rates of parent and leached catalysts as functions of areal CUS concentrations. For the leached samples, a direct linear dependence of the rates was observed for both reaction pathways, DDS and HYD, substantiating the absence of accessible, inactive NiS_x phases (i.e., they are located at inaccessible spaces as discussed earlier) that would distort the linearity. This suggests that the turnover frequency, based on total CUS, was identical for these samples, the one for DDS (70 $hour^{-1}$) being about a factor of 2 lower than for HYD (140 $hour^{-1}$). Similarly, CUS-normalized turnover frequencies were also estimated for the DDS and HYD routes over a sulfided Ni-Mo/Al_2O_3 catalyst (with a similar average slab length but a lower stacking degree than the bulk sulfides; see table S5). The turn-over frequency (TOF) of DDS was 97 $hour^{-1}$, comparable to that obtained on bulk sulfides, whereas the TOF of HYD was only 9 $hour^{-1}$, which was about 15 times smaller than that on bulk sulfides. The results suggest that the intrinsic catalytic activity of sites for DDS is rather insensitive to the variations in the geometric and electronic properties of the sulfide phase when changing the support (Al_2O_3 or the sulfide itself). In contrast, sites active for HYD appear to have a much greater structure sensitivity arising from support-induced variations in the ability to stabilize SH groups (originating from CUS) and the intrinsic activity of SH in mediating H-addition. We tentatively attribute this to the absence of Mo-O-Al linkages, leading to a higher polarity of metal-sulfur bonds and, thus, to an increased stability and concentration of SH groups. Apart from these considerations, it is worth noting that differences in stacking likely also contribute to the enhanced HYD activity of bulk sulfides (*20*). In particular, it is expected that flat adsorption of DBT (via dispersive interactions with the π-aromatic system) is possible on the multilayered sulfides while being at least unfavorable on monolayer-dominated Ni-Mo/Al_2O_3 (table S5).

Unpromoted MoS_2 exhibited a substantially smaller areal concentration of CUS, consistent with its greater metal-sulfur bond strength (>160 kJ mol^{-1}) than those in NiS_x (<100 kJ mol^{-1}) and the Ni-Mo-S phase (120 to 130 kJ mol^{-1}) (*3*). While the much higher activity of Ni-Mo catalysts compared to that of MoS_2 is well documented in the literature on HDS, we notice here that the difference in the TOFs between nonpromoted Mo sites and promoted sites was substantially smaller for the HYD pathway than for the DDS pathway (Fig. 5, B and C). In this connection, we note that TOFs of HYD of aromatics, e.g., BP (*41*), decrease in a much less pronounced manner than TOFs of desulfurization reactions, with M-S bond energies increasing beyond the optimal values (120 to 140 kJ mol^{-1}), i.e., going from Ni-MoS_2 to MoS_2. These observations seem compatible with the consideration that H-addition rates are jointly affected by M-S and S-H bond properties, in contrast to the rates of direct C-S cleavage that are mainly determined by the nature of M-S bonds (*3*).

CONCLUSIONS

Acid treatment removes a large fraction of NiS_x from Ni-Mo sulfide catalysts, leading to highly active materials, whose activity depends solely on the concentration of active sites consisting of CUS and SH groups. While most of the Ni after such treatment is incorporated in the Ni-Mo-S phase, the remaining fraction of NiS_x exists in the interior of secondary MoS_2 structures.

Unblocking of previously covered (sterically inaccessible) active sites and elimination of catalytically inert mass jointly increase HDS rates. After leaching, all Ni-Mo sulfides show the same TOF (CUS-normalized) for DDS and HYD (70 and 140 $hour^{-1}$, respectively, at 330°C). The rate of the HYD pathway is substantially higher on bulk Ni-Mo sulfides than that observed on the Al_2O_3-supported catalyst, which showed much higher selectivity to DDS (~90%). The relative rates for the two pathways are not affected by acid treatment, implying that uncovered sites have the same properties as those accessible in the parent bulk sulfides. The DDS turnover frequencies were nearly identical for bulk and supported Ni-Mo sulfides. Therefore, we conclude that reaction pathways for DDS are insensitive to support effects.

However, the HYD turnover frequency on the CUS-related active sites of bulk sulfides were more than an order of magnitude higher than that obtained for Al_2O_3-supported Ni-Mo sulfide catalysts. At present, we note two possible explanations for this unusually high rate. On the one hand, the absence of sulfide-Al_2O_3 interactions leads to a lower averaged Sanderson electronegativity and a higher

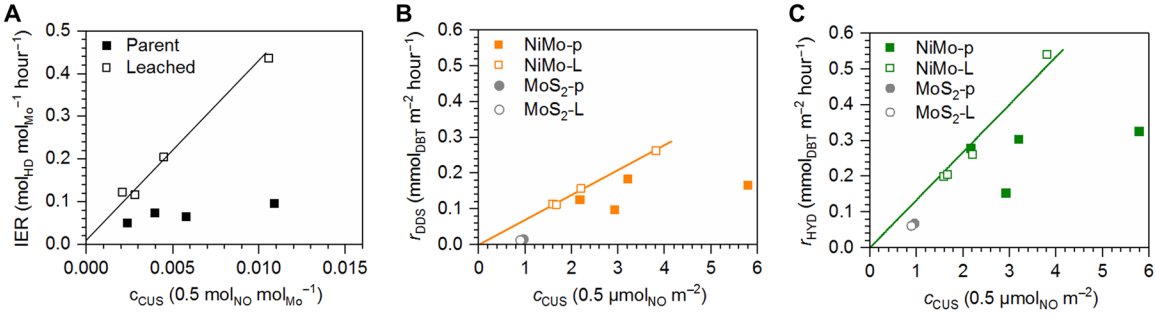

Fig. 5. Correlations between the reaction rates, IER, and the total CUS concentration. (**A**) IER as a function of total CUS concentration (normalized to total Mo content) as determined by NO chemisorption on parent (closed symbols) and leached catalysts (open symbols). Note that the factor 0.5 on the *x* axis results from assuming dinitrosyl adsorption at Ni-associated edge sites. (**B**) Initial DDS rate and (**C**) initial HYD rate normalized to surface area as a function of total CUS surface density in parent (closed symbols) and leached catalysts (open symbols).

polarity of the metal-sulfur bonds, altering the bonding of the reactants and the stabilization of reactive intermediates as well as the concentration of SH groups. On the other hand, we would like to point to the substantial morphological differences, in particular, stacking degree, and their implications for reactant adsorption. While these hypotheses require more investigations, the present study shows a promising guideline to maximize the catalytic activity in Ni-Mo-S–based catalysts especially for the HYD pathway, which is of central importance for the HDS of very heavy feedstocks.

MATERIALS AND METHODS

Catalyst preparation

Mixed metal oxide precursors were synthesized by hydrothermal reaction (*15*) of molybdenum(VI) oxide (MoO_3; Sigma; 99.5%) and nickel(II) carbonate hydroxide tetrahydrate [2 $Ni(CO_3)_2$·3 $Ni(OH)_2$·4 H_2O; Aldrich; 45.0 to 52.5% Ni] in a polytetrafluoroethylene (PTFE)–lined, stainless steel autoclave of 80-ml volume. Mo oxide was suspended in 50 ml of deionized water followed by the addition of Ni carbonate. The following amounts of Mo oxide and Ni-carbonate were used for NiMo-1, NiMo-2, NiMo-3, and NiMo-4: 1.92 and 0.82 g, 1.73 and 0.98 g, 1.44 and 1.22 g, and 1.15 and 1.47 g, respectively. After sealing the vessel, the reaction mixture was heated in a rotatory furnace (30 rpm) at a rate of about 10°C min^{-1} to 175°C and kept at this temperature for 17 hours. The autoclave was cooled to room temperature in a water bath and the solid material separated by filtration. After drying at 120°C (in air) for 12 hours, the yellow-greenish precipitate was ground to a fine powder and pressed into pellets of 255 to 350 μm diameter.

For sulfidation, about 500 mg of oxidic precursor was mixed with 1.5 g of SiC (ESK; 63 to 90 μm) and placed in a glass-coated, stainless steel tubular reactor of 4 mm internal diameter. The material was then dried for 1 hour at 120°C (ramp: 1°C min^{-1}) under nitrogen flow at ambient pressure (100 ml min^{-1} g_{cat}^{-1}). Subsequently, nitrogen was replaced by hydrogen (200 ml min^{-1} g_{cat}^{-1}) and the pressure increased to 2.0 MPa. At the same time, a solution of DMDS (dimethyl disulfide; Aldrich; 99%) in decalin (Merck; 99%), adjusted to contain 8 weight % (wt %) sulfur, was introduced into the reactor at a rate of 0.4 ml min^{-1} g_{cat}^{-1} and maintained until the end of the sulfidation procedure. During sulfidation, temperature was increased from 120° to 250°C at a rate of 1°C min^{-1} and kept at this temperature for 4 hours. This was followed by a final heating phase at 350°C (1°C min^{-1}) for 2 hours. The gas/liquid flow and the pressure were maintained until the reactor was cooled to room temperature. The reactor was then successively purged with toluene, hexane, and nitrogen to fully remove any residues of the sulfidation feed. Last, the sulfided catalyst pellets were separated by sieving and stored under nitrogen until use. Catalyst samples denoted as "parent" (suffix "-p") were not treated any further.

In addition to the mixed Ni-Mo sulfides, MoS_2 and Ni_3S_2 reference samples were included in the study. MoS_2 was prepared by dissolving 8.29 g of ammonium heptamolybdate tetrahydrate [$(NH_4)_6Mo_7O_{24}$·4 H_2O; Merck, extra pure] in 40 ml of water and adding 65 ml of aqueous ammonium sulfide solution [20 to 24 wt % $(NH_4)_2S$; Aldrich; 99%]. The mixture was stirred at 60°C for 1 hour and then cooled in ice for 3 hours. The red crystals of ammonium tetrathiomolybdate [$(NH_4)_2MoS_4$] were washed successively with cold water and cold acetone and then dried in ambient air overnight at room temperature. The material was ground and pelletized to particles of 255 to 350 μm diameter. MoS_2 was obtained by subsequent heating in hydrogen (100 ml min^{-1} g^{-1}) to 400°C at a rate of 3 K min^{-1} and holding this temperature for 4 hours.

Ni_3S_2 was prepared by dissolving 10.9 g of Ni(II) nitrate hexahydrate [$Ni(NO_3)_2$·6 H_2O; Alfa Aesar; 99.9985% (metals basis)] in 150 ml of water and slowly (1.5 hours) adding a solution of 6.00 g of sodium sulfide nonahydrate [Na_2S·9 H_2O; Aldrich; 99.99% (metals basis)] in 150 of ml water. The black precipitate was successively washed with water and acetone, dried overnight in vacuum, and pelletized to particles of 255 to 350 μm diameter. To obtain Ni_3S_2, the material was first heated to 300°C at a ramp rate of 3.3°C min^{-1} in H_2S (10% in H_2, 40 ml min^{-1} g^{-1}) and held at this temperature for 3 hours. Then, the flow was changed to hydrogen (40 ml min^{-1} g^{-1}), and the temperature was held for further 4 hours before naturally cooling to room temperature.

For acid treatment, a portion of the parent sulfide, approximately 200 mg, was placed in a wide beaker and the pellets were fully covered with about 10 ml of concentrated hydrochloric acid (Fluka; 37%, fuming, trace analysis grade). After 1 hour at room temperature, the greenish solution (colorless in the case of MoS_2) was decanted and discarded before a new portion of HCl was added to the pellets. This procedure was repeated three times per sample. Subsequently, the pellets were washed several times with water and finally with acetone before being left to dry at room temperature in ambient air overnight. Samples subjected to acid treatment are denoted as "leached" (suffix "-L").

Characterization

Elemental analysis of sulfided catalyst samples was performed by acidic digestion and subsequent photometric determination using a Shimadzu UV-160 photometer (for Ni, Mo). An Elementar Vario EL combustion analyzer was used for C,H,N,S analysis. Textural parameters were determined by nitrogen physisorption using an automated PMI Sorptomatic 1990 instrument at liquid nitrogen temperature. The samples were outgassed in vacuum at 120°C for 2 hours before adsorption. Specific surface areas were obtained by applying Brunauer-Emmett-Teller (BET) theory on the adsorption branch of the isotherms.

XRD was performed on a Philips X'Pert Pro diffractometer in Bragg-Brentano geometry using Cu-Kα radiation ($K\alpha_2/K\alpha_1$ = 0.5) operating at 45 kV and 40 mA. XRD measurements were carried out using a rotating zero-diffraction plate (single crystal of Si cut in special orientation). The step size was fixed to 0.017°θ with a dwell time of 115 ms per step. Crystallite sizes were determined using the Scherrer equation (see Supplementary Methods).

SEMs were obtained on a JEOL JSM-7500F instrument using secondary electron detection and operating at an acceleration voltage of 1.0 kV. TEM was performed on a JEOL JEM-2011 instrument at an acceleration voltage of 120 kV. Before analysis, the samples were suspended in absolute ethanol and dispersed ultrasonically before being deposited on a carbon-coated copper mesh.

Hydrogen-deuterium isotopic exchange was carried out at 100°C, and ambient pressure in a fixed-bed reactor, which was attached to a mass spectrometer. The catalyst pellets, typically 100 mg, were placed in a quartz tube of 4 mm inner diameter and then resulfided in a flow of H_2S (10% in H_2, 100 ml min^{-1} g^{-1}) by heating to 320°C (5°C min^{-1}) and holding this temperature for 2 hours. During this procedure, desorption of water [mass/charge ratio (m/z) = 18] was noticed but no measurable uptake of H_2S. After naturally cooling

to room temperature, a 1:1 mixture of H_2 and D_2 in N_2 was introduced into the reactor at varying total flow rates, while the ratio of the reactants was kept constant (17 volume % H_2, 17 volume % D_2, balance: N_2). HD concentration was monitored using the signal at $m/z = 3$. Initial HD formation rate was calculated at conversions <5% (H_2 or D_2) according to the following equation

$$r_{HD} = \chi_{HD} \cdot \frac{\dot{n}_{total}}{m_{cat}} \quad (1)$$

where χ is the molar fraction of HD, $\dot{n}_{total}$ is the total molar flow to the reactor, and m_{cat} is the mass of the catalyst.

NO chemisorption was carried out at ambient temperature and pressure following H_2-D_2 isotopic exchange experiments. While under constant He flow (100 ml min^{-1} g^{-1}), a pulse of NO (10% in He) was dosed into the reactor every 30 min by an automated valve (24 pulses in total, 6.82 µmol of NO per pulse). Specific NO uptakes were calculated by subtracting each residual peak area (i.e., NO not adsorbed) from the averaged peak area after saturation with NO and adding up the differences. NO concentration was monitored using the signal at $m/z = 30$.

X-ray absorption spectra were collected at the P65 XAFS beamline at the PETRA III synchrotron light source at DESY (Deutsches Elektronen-Synchrotron) (Hamburg, Germany). All data were recorded in fluorescence yield mode at the Ni K-edge at 8333 eV using an Si (111) monochromator. Energy alignment was performed by using a metallic Ni foil placed behind the sample and measured at the same time (in transmission mode). The sulfided catalyst was diluted with boron nitride and placed in a quartz capillary of 1 mm inner diameter. To ensure complete sulfidation of the catalysts' surface, the capillary was then heated from ambient temperature to 350°C at a rate of 5°C min^{-1} and held at this temperature for 1 hour. A heated gas blower (Oxford Laboratories) was used for this purpose. Before resulfidation, the capillary with the catalyst was purged with He, after which the flow was changed to H_2S (10% in H_2) and maintained during the whole procedure. The spectra (8133 to 8883 eV) were recorded after cooling down to 30°C and purging with He. Four spectra were collected per sample, normalized to the absorption edge height, and averaged before further data treatment. Energy-dependent edge height normalization, merging of spectra, background subtraction, and self-absorption correction were done using built-in capabilities of the ATHENA software package (*42*). Absorption edge height was determined as the difference of extrapolated pre-edge and post-edge intensities. The k^3-weighed spectra were then Fourier-transformed in the k-range of 3 to 10.5 $Å^{-1}$ (parent) or 3 to 12.4 $Å^{-1}$ (leached) and multiplied with a window function to avoid cutoff effects [Hann function (*43*) of width 1 $Å^{-1}$]. The EXAFS was fitted using the ARTEMIS software package (*42*) with included IFEFFIT (*44*) functionality. Further details of the fitting model are explained in detail in the Supplementary Methods.

Kinetic measurements

In a typical run, about 25 mg of sulfided catalyst pellets (parent or leached) was mixed with 1 g of SiC (63 to 90 µm) and placed in the tubular reactor described above. The reaction mixture was then fed to the reactor together with hydrogen at a total pressure of 5.0 MPa and a gas to liquid ratio of 500 (volumetric base). The liquid feed consisted of 1 wt % DBT (Aldrich; 99%) in decalin and 0.15 wt % DMDS (= 1000 ppm S). In temperature variation experiments, the weight hourly space velocity (WHSV) was kept constant at 1.0 $hour^{-1}$. Where necessary (contact time variation), the WHSV was changed by adjusting the flow rate of liquid and gaseous reactants while keeping their ratio constant. After heating to reaction temperature (330°C at 1°C min^{-1}), the catalyst was stabilized for a period of 12 hours, after which liquid samples were collected in periodic intervals (typically three samples per operating condition). The stability of the catalyst was verified by comparing the conversion at the beginning and at the end of one catalytic run at identical conditions.

Liquid reaction products were analyzed offline in an HP 6890 gas chromatograph equipped with a flame ionization detector and an HP-1701 fused silica capillary column (14% cyanopropyl-phenyl-methylpolysiloxane; 60 m by 250 µm by 0.25 µm). Quantification was performed by external calibration with solutions of reference compounds of known concentration. The carbon balance across the reactor was 97% or better in the studied range of conversions (typically <40%). Conversion was calculated on the basis of reacted DBT according to the following equation

$$X = \frac{c_{DBT}(inlet) - c_{DBT}(outlet)}{c_{DBT}(inlet)} \cdot 100\% \quad (2)$$

where $\dot{n}_{DBT}$ is the concentration of DBT at the reactor inlet and outlet, respectively. The selectivity for the DDS pathway was based on the BP product, while the selectivity for the HYD pathway was based on the sum of 4HDBT, CHB, and BCH. Selectivities were calculated as follows

$$S_{DDS} = \frac{c_{BP}}{c_{BP} + c_{4HDBT} + c_{CHB} + c_{BCH}} \cdot 100\% \quad (3)$$

$$S_{HYD} = \frac{c_{4HDBT} + c_{CHB} + c_{BCH}}{c_{BP} + c_{4HDBT} + c_{CHB} + c_{BCH}} \cdot 100\% \quad (4)$$

where c_i is the concentration of the respective product at the outlet of the reactor. Rates were directly calculated from selectivity and conversion according to the following equations

$$r_{DBT} = \frac{X}{100\%} \cdot \frac{\dot{n}_{DBT}(inlet)}{m_{cat}} \quad (5)$$

$$r_{DDS} = \frac{S_{DDS}}{100\%} \cdot \frac{X}{100\%} \cdot \frac{\dot{n}_{DBT}(inlet)}{m_{cat}} \quad (6)$$

$$r_{HYD} = \frac{S_{HYD}}{100\%} \cdot \frac{X}{100\%} \cdot \frac{\dot{n}_{DBT}(inlet)}{m_{cat}} \quad (7)$$

where X and S_i are the conversion and selectivity, respectively; $\dot{n}_{DBT}$ (inlet) is the molar flow of DBT at the reactor inlet; and m_{cat} is the catalyst mass. Note that the resulting rates are considered as initial rates, irrespective of conversion, because DBT consumption followed an apparent zero-order dependence in DBT. Further, DDS and HYD selectivities were not dependent on conversion (see fig. S7).

SUPPLEMENTARY MATERIALS

Supplementary material for this article is available at http://advances.sciencemag.org/cgi/content/full/6/19/eaax5331/DC1

REFERENCES AND NOTES

1. R. Prins, Hydrotreating, in *Handbook of Heterogeneous Catalysis*, G. Ertl, H. Knözinger, F. Schüth, J. Weitkamp, Eds. (Wiley-VCH, 2008), vol. 1, chap. 13.2, pp. 2695–2718.
2. H. Topsøe, B. S. Clausen, F. E. Massoth, Hydrotreating catalysis, in *Catalysis: Science and Technology*, J. R. Anderson, M. Boudart, Eds. (Springer, 1996), vol. 11, pp. 1–269.
3. H. Toulhoat, P. Raybaud, *Catalysis by Transition Metal Sulphides: From Molecular Theory to Industrial Application* (Editions Technip, 2013).

4. S. Eijsbouts, J. J. L. Heinerman, H. J. W. Elzerman, MoS_2 structures in high activity hydrotreating catalysts. II. Evolution of the active phase during the catalyst life cycle. Deactivation model. *Appl. Catal. A* **105**, 69–82 (1993).
5. S. Eijsbouts, X. Li, J. Bergwerff, J. Louwen, L. Woning, J. Loos, Nickel sulfide crystals in Ni-Mo and Ni-W catalysts: Eye-catching inactive feature or an active phase in its own right? *Catal. Today* **292**, 38–50 (2017).
6. S. Albersberger, J. Hein, M. W. Schreiber, S. Guerra, J. Han, O. Y. Gutiérrez, J. A. Lercher, Simultaneous hydrodenitrogenation and hydrodesulfurization on unsupported Ni-Mo-W sulfides. *Catal. Today* **297**, 344–355 (2017).
7. J. Bachelier, J. Duchet, D. Cornet, Hydrodesulfurization with NiO-Al_2O_3 catalysts—Nature of active phase. *Bull. Soc. Chim. Fr. I*, 112–118 (1978).
8. J. Bachelier, J. Duchet, D. Cornet, Hydrodesulfurization over NiO-Al_2O_3 catalysts—Effect of catalysts treatment on the active phase. *Bull. Soc. Chim. Fr. I*, 221–228 (1979).
9. J. Bachelier, M. J. Tilliette, J. C. Duchet, D. Cornet, Surface phases in sulfided Ni-Mo/Al_2O_3 catalysts. *J. Catal.* **87**, 292–304 (1984).
10. M. V. Landau, L. I. Nikulina, B. K. Nefedov, A. A. Slinkin, Effect of nickel on the hydrogenating activity of MoS_2. *React. Kinet. Catal. Lett.* **25**, 115–119 (1984).
11. W. Luo, H. Shi, E. Schachtl, O. Y. Gutiérrez, J. A. Lercher, Active sites on nickel-promoted transition-metal sulfides that catalyze hydrogenation of aromatic compounds. *Angew. Chem. Int. Ed.* **57**, 14555–14559 (2018).
12. O. Glemser, E. Schwarzmann, Nickel, Kobalt, in *Handbuch der Präparativen Anorganischen Chemie*, G. Brauer, Ed. (Enke Verlag, 1981), vol. 3, chap. 29, pp. 1659–1703.
13. J. J. Berzelius, Beitrag zur näheren Kenntniss des Molybdäns. *Ann. Phys.* **82**, 369–392 (1826).
14. J. V. Sanders, K. C. Pratt, The relationship of structure and activity of NiMo sulfides to composition of the precursor oxides. *J. Catal.* **67**, 331–347 (1981).
15. S. Eijsbouts, S. Miseo, F. L. Plantenga, S. L. Soled, Hydroprocessing using hydrothermally-prepared bulk multimetallic catalysts, US7686943B2 (2010).
16. J. Hein, A. Hrabar, A. Jentys, O. Y. Gutiérrez, J. A. Lercher, γ-Al_2O_3-supported and unsupported (Ni)MoS_2 for the hydrodenitrogenation of quinoline in the presence of dibenzothiophene. *ChemCatChem* **6**, 485–499 (2014).
17. J. Hein, O. Y. Gutiérrez, S. Albersberger, J. Han, A. Jentys, J. A. Lercher, Towards understanding structure–activity relationships of Ni–Mo–W sulfide hydrotreating catalysts. *ChemCatChem* **9**, 629–641 (2017).
18. E. Schachtl, L. Zhong, E. Kondratieva, J. Hein, O. Y. Gutiérrez, A. Jentys, J. A. Lercher, Understanding Ni promotion of MoS_2/γ-Al_2O_3 and its implications for the hydrogenation of phenanthrene. *ChemCatChem* **7**, 4118–4130 (2015).
19. V. V. Atuchin, T. A. Gavrilova, V. G. Kostrovsky, L. D. Pokrovsky, I. B. Troitskaia, Morphology and structure of hexagonal MoO_3 nanorods. *Inorg. Mater.* **44**, 622 (2008).
20. F. B. Garreau, H. Toulhoat, S. Kasztelan, R. Paulus, Low-temperature synthesis of mixed NiMo sulfides: Structural, textural and catalytic properties. *Polyhedron* **5**, 211–217 (1986).
21. S. M. A. M. Bouwens, D. C. Koningsberger, V. H. J. De Beer, S. P. A. Louwers, R. Prins, Exafs study of the local structure of Ni in Ni-MoS_2/C hydrodesulfurization catalysts. *Catal. Lett.* **5**, 273–283 (1990).
22. J. Hein, O. Y. Gutiérrez, E. Schachtl, P. H. Xu, N. D. Browning, A. Jentys, J. A. Lercher, Distribution of metal cations in Ni-Mo-W sulfide catalysts. *ChemCatChem* **7**, 3692–3704 (2015).
23. S. P. A. Louwers, R. Prins, Ni EXAFS studies of the Ni-Mo-S structure in carbon-supported and alumina-supported Ni-Mo catalysts. *J. Catal.* **133**, 94–111 (1992).
24. W. Niemann, B. S. Clausen, H. Topsøe, X-ray absorption studies of the Ni environment in Ni-Mo-S. *Catal. Lett.* **4**, 355–363 (1990).
25. H. Topsøe, B. S. Clausen, N.-Y. Topsøe, E. Pedersen, W. Niemann, A. Müller, H. Bögge, B. Lengeler, Inorganic cluster compounds as models for the structure of active sites in promoted hydrodesulphurization catalysts. *J. Chem. Soc. Faraday Trans. 1* **83**, 2157–2167 (1987).
26. E. Krebs, B. Silvi, P. Raybaud, Mixed sites and promoter segregation: A DFT study of the manifestation of Le Chatelier's principle for the Co(Ni)MoS active phase in reaction conditions. *Catal. Today* **130**, 160–169 (2008).
27. E. Krebs, A. Daudin, P. Raybaud, A DFT study of CoMoS and NiMoS catalysts: From nano-crystallite morphology to selective hydrodesulfurization. *Oil Gas Sci. Technol. Rev. IFP* **64**, 707–718 (2009).
28. K. Marchand, C. Legens, D. Guillaume, P. Raybaud, A rational comparison of the optimal promoter edge decoration of HDT NiMoS vs CoMoS catalysts. *Oil Gas Sci. Technol. Rev. IFP* **64**, 719–730 (2009).
29. S. Houssenbay, S. Kasztelan, H. Toulhoat, J. P. Bonnelle, J. Grimblot, Nature of the different nickel species in sulfided bulk and alumina-supported nickel-molybdenum hydrotreating catalysts. *J. Phys. Chem.* **93**, 7176–7180 (1989).
30. M. Houalla, N. K. Nag, A. V. Sapre, D. H. Broderick, B. C. Gates, Hydrodesulfurization of dibenzothiophene catalyzed by sulfided CoO-MoO_3/γ-Al_2O_3: The reaction network. *AlChE J.* **24**, 1015–1021 (1978).
31. G. H. Singhal, R. L. Espino, J. E. Sobel, Hydrodesulfurization of sulfur heterocyclic compounds: Reaction mechanisms. *J. Catal.* **67**, 446–456 (1981).
32. M. J. Girgis, B. C. Gates, Reactivities, reaction networks, and kinetics in high-pressure catalytic hydroprocessing. *Ind. Eng. Chem. Res.* **30**, 2021–2058 (1991).
33. H. Wang, R. Prins, Hydrodesulfurization of dibenzothiophene, 4,6-dimethyldibenzothiophene, and their hydrogenated intermediates over Ni–MoS_2/γ-Al_2O_3. *J. Catal.* **264**, 31–43 (2009).
34. M. Egorova, R. Prins, Hydrodesulfurization of dibenzothiophene and 4,6-dimethyldibenzothiophene over sulfided NiMo/γ-Al_2O_3, CoMo/γ-Al_2O_3, and Mo/γ-Al_2O_3 catalysts. *J. Catal.* **225**, 417–427 (2004).
35. Y. Sun, R. Prins, Mechanistic studies and kinetics of the hydrodesulfurization of dibenzothiophene on Co–MoS_2/γ–Al_2O_3. *J. Catal.* **267**, 193–201 (2009).
36. M. Daage, R. R. Chianelli, Structure-function relations in molybdenum sulfide catalysts: The "rim-edge" model. *J. Catal.* **149**, 414–427 (1994).
37. N. Y. Topsøe, H. Topsøe, FTIR studies of Mo/Al_2O_3-based catalysts: II. Evidence for the presence of SH groups and their role in acidity and activity. *J. Catal.* **139**, 641–651 (1993).
38. R. Candia, B. S. Clausen, H. Topsøe, On the role of promoter atoms in unsupported hydrodesulfurization catalysts: Influence of preparation methods. *Bull. Soc. Chim. Belg.* **90**, 1225–1232 (1981).
39. J. V. Lauritsen, S. Helveg, E. Lægsgaard, I. Stensgaard, B. S. Clausen, H. Topsøe, F. Besenbacher, Atomic-scale structure of Co–Mo–S nanoclusters in hydrotreating catalysts. *J. Catal.* **197**, 1–5 (2001).
40. E. Schachtl, E. Kondratieva, O. Y. Gutiérrez, J. A. Lercher, Pathways for H_2 activation on (Ni)-MoS_2 catalysts. *J. Phys. Chem. Lett.* **6**, 2929–2932 (2015).
41. M. Lacroix, N. Boutarfa, C. Guillard, M. Vrinat, M. Breysse, Hydrogenating properties of unsupported transition metal sulphides. *J. Catal.* **120**, 473–477 (1989).
42. B. Ravel, M. Newville, Athena, Artemis, Hephaestus: Data analysis for X-ray absorption spectroscopy using IFEFFIT. *J. Synchrotron Radiat.* **12**, 537–541 (2005).
43. R. B. Blackman, J. W. Tukey, The measurement of power spectra from the point of view of communications engineering—Part I. *Bell Syst. Tech. J.* **37**, 185–282 (1958).
44. M. Newville, IFEFFIT: Interactive XAFS analysis and FEFF fitting. *J. Synchrotron Radiat.* **8**, 322–324 (2001).
45. S. I. Zabinsky, J. J. Rehr, A. Ankudinov, R. C. Albers, M. J. Eller, Multiple-scattering calculations of X-ray-absorption spectra. *Phys. Rev. B* **52**, 2995–3009 (1995).
46. M. Fleet, Structure of godlevskite, Ni_9S_8. *Acta Crystallogr. C* **43**, 2255–2257 (1987).
47. I. Søtofte, The crystal structure of tetraphenylphosphonium bis(tetrathiomolybdato) nickelate(II). *Acta Chem. Scand.* **30A**, 157–162 (1976).
48. L. Brillouin, *Science and Information Theory* (Dover Publications, 1956).
49. P. R. Bevington, D. K. Robinson, *Data Reduction and Error Analysis for the Physical Sciences* (McGraw-Hill, 1992).
50. B. Ravel, Quantitative EXAFS Analysis, in *X-Ray Absorption and X-Ray Emission Spectroscopy: Theory and Applications*, J. van Bokhoven, C. Lamberti, Eds. (Wiley, 2016), pp. 281–302.
51. E. Peters, Direct Leaching of sulfides: Chemistry and applications. *Metall. Trans. B* **7**, 505–517 (1976).
52. M. Landau, D. Agievskii, A. Slinkin, M. Kipnis, L. Alekseenko, E. Fedorovskaya, L. Pavlova, T. Kucherovat, Active structures of the product of sulfiding of nickel molybdate. Hydrogenation of aromatic hydrocarbons. *Kinet. Catal.* **23**, 5747692 (1983).
53. L. Gurvitsch, Physicochemical attractive force. *J. Phys. Chem. Russ.* **47**, 805–827 (1915).
54. N.-Y. Topsøe, H. Topsøe, Characterization of the structures and active sites in sulfided CoMo/Al_2O_3 and Ni/$MoAl_2O_3$ catalysts by NO chemisorption. *J. Catal.* **84**, 386–401 (1983).
55. R. P. Silvy, F. Delannay, P. Grange, B. Delmon, Effect of the activation conditions on the structure and catalytic activity of a CoMo/γ-Al_2O_3 hydrodesulfurization catalyst. *Polyhedron* **5**, 195–198 (1986).
56. A. L. Agudo, F. J. Gil Llambías, J. M. D. Tascón, J. L. G. Fierro, Characterization of Sulfided Ni-Mo/γ-Al_2O_3 Catalysts by O_2 and NO Chemisorption. *Influence of the Method of Preparation. Bull. Soc. Chim. Belg.* **93**, 719–726 (1984).
57. N.-Y. Topsøe, H. Topsøe, O. Sørensen, B. S. Clausen, R. Candia, IR and AEM evidence for the edge location of the promoter atoms in Co-Mo-S type structures. *Bull. Soc. Chim. Belg.* **93**, 727–734 (1984).
58. N.-Y. Topsøe, A. Tuxen, B. Hinnemann, J. V. Lauritsen, K. G. Knudsen, F. Besenbacher, H. Topsøe, Spectroscopy, microscopy and theoretical study of NO adsorption on MoS_2 and Co–Mo–S hydrotreating catalysts. *J. Catal.* **279**, 337–351 (2011).
59. F. Caron, M. Rivallan, S. Humbert, A. Daudin, S. Bordiga, P. Raybaud, Active sites speciation of supported CoMoS phase probed by NO molecule: A combined IR and DFT study. *J. Catal.* **361**, 62–72 (2018).
60. L. Portela, P. Grange, B. Delmon, The adsorption of nitric oxide on supported Co-Mo hydrodesulfurization catalysts: A review. *Catal. Rev.* **37**, 699–731 (1995).

Acknowledgments: We thank L. Meyer (support in catalyst preparation, characterization, and kinetic measurements), W. Luo (support in kinetic measurements), X. Hecht (BET), U. Sanyal and A. Ehrmaier (TEM), and T. Ikuno (SEM). We also thank R. Prins for his careful reading of the

manuscript and helpful suggestions. We are especially grateful to A. Kuperman and A. Brait for fruitful discussions. XAS measurements were carried out at the PETRA III synchrotron light source at DESY, a member of the Helmholtz Association (HGF). We thank E. Welter and staff members for assistance in using the P65 XAFS beamline. **Funding:** This work of A.J. was supported by BMBF under the project MatDynamics (Verbundprojekt 05K13W03). Parts of this work were funded by the Chevron Energy Technology Company (contract number Chevron Inc.—TU München: CW 776910 period: 15 May 2014 to 14 May 2017). **Author contributions:** M.F.W. and O.Y.G. conceived the initial idea; H.S. and J.A.L. directed the research; M.F.W. conducted most of the described experiments, material syntheses, and characterization. A.J. contributed to EXAFS data evaluation. M.F.W., O.Y.G., H.S., and J.A.L. wrote the manuscript. All authors discussed the results and commented on the manuscript. **Competing interests:** The authors declare that they have no competing interests. **Data and materials availability:** All data needed to evaluate the conclusions in the paper are present in the paper and/or the Supplementary Materials. Additional data related to this paper may be requested from J.A.L. (johannes.lercher@ch.tum.de).

Submitted 1 April 2019
Accepted 26 February 2020
Published 8 May 2020
10.1126/sciadv.aax5331

Citation: M. F. Wagenhofer, H. Shi, O. Y. Gutiérrez, A. Jentys, J. A. Lercher, Enhancing hydrogenation activity of Ni-Mo sulfide hydrodesulfurization catalysts. *Sci. Adv.* **6**, eaax5331 (2020).

Science Advances

Enhancing hydrogenation activity of Ni-Mo sulfide hydrodesulfurization catalysts

Manuel F. Wagenhofer, Hui Shi, Oliver Y. Gutiérrez, Andreas Jentys and Johannes A. Lercher

Sci Adv **6** (19), eaax5331.
DOI: 10.1126/sciadv.aax5331